Optical diagnostics study of air flow and powder fluidisation in Nexthaler®

Part I: Studies with Lactose Placebo Formulation

Pasquali I.[1], Merusi C.[1], Brambilla G.[1], Long E.J.[2], Hargrave G.K.[2], Versteeg H.K.[2†]

[1] Chiesi Farmaceutici S.p.A., Parma, Italy

[2] Wolfson School of Mechanical and Manufacturing Engineering, Loughborough University, Loughborough, United Kingdom

[†] Corresponding author:

Wolfson School of Mechanical and Manufacturing Engineering, Loughborough University, Loughborough, LE11 3TU, United Kingdom.

Tel: +44(0)1509-227528; Email: H.K.Versteeg@Lboro.ac.uk

Abstract

Effective drug delivery to the lungs by a DPI device requires the air-stream through the device to have sufficient power to aerosolise the powder. Furthermore, sufficient turbulence must be induced, along with particle-wall and particle-particle collisions, in order to de-aggregate small drug particles from large carrier particles. As a result, the emitted and the fine particle doses produced by many commercially available DPI devices tend to be strongly affected by the natural inter-patient variability of the inhaled air flow. The Nexthaler® is a multi-dose breath-actuated dry-powder inhaler with minimum drug delivery-flow rate dependency and incorporating a dose protector. The actuation mechanism of the dose-protector ensures that the dose is only exposed to the inhaled air flow if the flow has sufficient power to cause complete aerosolisation. For this study, a proprietary lactose placebo powder blend was filled into “transparent “ Nexthalers® to allow application of high-speed imaging and particle image velocimetry (PIV) techniques to successfully interrogate and reveal details of the powder entrainment and emission processes coupled with characterisation of the flow environment in the vicinity of the mouthpiece exit.

The study showed that fluidisation of the bulk of the powder occurs very quickly (~20 ms) after withdrawal of the dose protector followed by powder emission from the device within ~50 ms thereafter. The bulk of the metered placebo dose was emitted within 100-200 ms. The visualisation study also revealed that a very small fraction of powder fines is emitted whilst the dose protector still covers the dosing cup as the flow rate through the device accelerates. The PIV results show that the flow exiting the device is highly turbulent with a rotating flow structure, which forces the particles to follow internal paths having a high probability of wall impacts, suggesting that the flow environment inside the Nexthaler® DPI will be very beneficial for carrier-drug de-aggregation.

Keywords: powder fluidization; dry powder inhaler; breath-actuated; optical diagnostics; high-speed imaging; particle image velocimetry; powder emission

1. Introduction

Dry powder inhalers (DPI) deliver therapeutic agents to the lungs and airways in the form of a powder aerosol. To achieve efficient delivery of these agents to the lungs, perceived wisdom suggests the aerodynamic particle size should range between 1 and 5 μm (Laube *et al.,* 2011), although it is arguable that sub-micron particles are also capable of lung deposition and retention, (Acerbi *et al.*, 2007, Church *et al.*, 2010, Kuna *et al.*, 2015). Micronised drug powders in these ranges tend to be very cohesive and, consequently, to ensure flowability during formulation manufacture, device filling, storage and use, drug particles are presented in the form of aggregates of micronized drug particles alone or of drug and coarse lactose carrier particles, (Newman and Busse, 2002).

Most of the DPI devices currently on the market are breath-actuated, single-dose or multi-dose DPIs (British National Formulary 68, 2014, EMC, 2015, Physician's Desk Reference, 2015). In these devices, the powder is aerosolised by the flow of air inhaled by the patient, which obviates the need for the patient to coordinate actuation/priming of the device and inhalation. However, as demonstrated in early work (Clark and Hollingsworth, 1993; Hindle and Byron, 1995; de Boer *et al.,* 1996), this advantage also has a well-known drawback, for many DPI systems, in that the resultant delivered and fine particle doses vary with the inhalation flow rate, which, in turn, depends on an individual patient's lung function and the device resistance. Staniforth (1995) studied the dependence of the fraction of a powder dose entrained by an air stream in a simple entrainment tube with circular cross-section, on flow velocity and the size of carrier particles. This work showed that partial fluidisation of the powder dose is initiated at lower air velocities, but complete fluidisation requires significantly higher velocities. Furthermore, complete aerosolisation takes place at lower velocities if the particles are larger. Clearly, the patient must be able to inhale with sufficient force to fluidise the powder-dose completely (Laube *et al.,* 2011). Moreover, in-vitro studies have shown that the emitted dose and the fine particle fraction of active drug emitted by the device depends on

72 the inhalation flow rate and its temporal profile (Everhard et al., 1997; Hawsksworth et al., 2000;
73 Chavan and Dalby, 2002).

74 Theories of powder fluidisation and de-aggregation (Dunbar *et al*. 1998, Finlay, 2001) propose that
75 shear fluidisation is responsible for entrainment of particles in the vicinity of a solid wall immersed in
76 a high speed boundary layer. Estimates of the fluid velocity required to initiate particle movement
77 were made on the basis of a balance between aerodynamic lift and drag forces vs. particle weight
78 and adhesion forces. Sweeney and Finlay (2007) gave details of a numerical study of the
79 aerodynamics of a sphere attached to a wall and immersed in a boundary layer under
80 hydrodynamic conditions that are representative of practical DPI flows; this work provided
81 interpolated closed-form relationships for the aerodynamic lift and drag coefficients that are useful
82 for accurate evaluations of the force balance. Voss and Finlay (2002) compared particle de-
83 aggregation in air flows with independent control of turbulence levels and mechanical impaction
84 conditions in a simplified entrainment tube test rig and a Diskhaler®. Laser-Doppler velocimetry
85 was used to measure turbulent flow velocities inside both systems. Their results showed that
86 turbulence in the air flow is the main variable that affects de-aggregation, an important finding for
87 subsequent device development. In separate work, Wang *et al.* (2004) studied Ventodisk® powder
88 fluidisation using normally impacting jet flows, as commonly found in commercial DPIs and reported
89 that the jet velocity, the amount of drug formulation loaded and the geometries of the jet and powder
90 dosing cup all affect fluidisation. Powder dispersion and drug de-aggregation were found to be
91 controlled by a combination of the following mechanisms: shear fluidisation, flow turbulence, jet
92 energy as well as particle-wall collisions. Zhou *et al.* (2010) studied fluidisation of lactose powders
93 with median particle sizes around 4 and 20 μm, with and without magnesium stearate in a
94 Monodose® (RS01 Plastiape) inhaler device. The study highlighted the role of powder bulk
95 characteristics and the potential of powder surface modification to improve aerosol performance,
96 reducing emitted drug dose dependence on the inhalation flow rate and improvement in drug de-
97 aggregation. The theoretical approach developed by Xu *et al.* (2010) for the study of particle
98 fluidisation in turbulent air flows within simplified entrainment tubes enabled predictions of drug fine-

particle fraction in the resultant aerosol cloud. Recent work by Xu and Hickey (2013) confirmed that predictions based on this theory show excellent agreement with the measured trends of fine-particle fractions as a function of air flow rate in commercial DPIs. Despite such investigations, for many widely prescribed products, there remains significant potential for poorly controlled interactions between the powder and inhaled air stream resulting from natural variations in the patterns of patients' inspiration and their different abilities to inhale with sufficient force. These factors can potentially lead to variations in the effectiveness of drug therapy delivered by means of dry-powder inhalers as a consequence of:

(i) incomplete powder fluidisation when a patient is unable to inhale sufficiently forcefully.
(ii) inconsistency of drug release from carrier vehicles due to variations of the strength of the inhaled air currents.

The exact details of the mechanism of powder fluidisation and subsequent drug release into the more complex air stream within commercial DPIs are still not well understood making it difficult to take a fundamental approach to DPI device design, which, consequently, proceeds largely on an empirical basis reliant on extensive use of cascade impaction testing (Friebel *et al.*, 2013). The challenges associated with sensing and measuring the rapid transient motion of dense particle-laden flows have been insurmountable until fairly recently. However, powerful optical diagnostic techniques are now available for imaging and measurements. One such technique, particle image velocimetry (PIV), was used by Ngoc *et al.* (2013) to study details of the flow fields and turbulence distribution in a de-agglomeration chamber of an idealised DPI. This yielded a deeper understanding of the flow mechanisms and geometrical factors controlling device performance.

In this paper we describe the use of optical diagnostics techniques, comprising high speed imaging coupled with PIV to study powder fluidisation and particle cloud emission from Nexthaler®, a multi-dose, breath-actuated, dry powder inhaler device approved for the delivery of drug powder formulations for the treatment of Asthma and COPD.

2. Materials and Methods

2.1 "Transparent" Nexthalers

The components of commercial Nexthalers®, (Corradi *et al.*, 2014), are machine or hand assembled from filled plastic pieces fabricated on multi-cavity tools. To allow the required internal optical access for this study, "transparent" versions were hand assembled from un-filled pieces, of otherwise identical material composition, fabricated using the identical moulding tools and conditions. For the data presented, two Nexthaler devices were used; one for the imaging testing (refilled as required) and one for the velocity measurements. The device incorporates a dose protector, which covers the metered mass of formulation, (dose), released when the device is primed prior to inhalation. It is designed to retract only when the suction produced by the inspiratory effort of the patient reaches the pre-set "trigger" value. As a consequence, the powder dose can only be exposed to a powerful inhaled air current, thereby ensuring its complete fluidisation and efficient dose emission.

2.2 Inhalation Powder Formulation

The powder reservoirs of part-assembled devices were hand-filled with 1.5 g of a proprietary lactose-excipient placebo blend, manufactured at commercial scale (Chiesi Farmaceutici, Parma) and the DPI assembly completed.

2.3 Optical Diagnostics Test Rig

2.3.1 Components

The experimental apparatus used for high-speed visualisation and measurement of the particle velocities within and emerging from a "transparent" Nexthaler® comprises a pneumatic suction system equipped with rapid response pressure and flow measurement instrumentation and optical systems. The apparatus, shown schematically in Figures 1-3, was assembled in-house utilising the following components.

A. Vacuum pump – Edwards Speedivac ED660

B. Control valve – Legris Stainless steel ball valve

C. 20 litre steel vacuum vessel

D. Sonic Restrictor – made in-house

E. Flow Control Valve – Legris Stainless steel ball valve

F. Rapid Switch Solenoid Controlled Ball Valve – Omal SR15 driven with 6 bar pressure

G. Variable Volume Unit – made in-house

H. Thermal Mass Flow Meter – Sierra 0-200 $sl.min^{-1}$ Accuracy: 1.0% of full scale

I. Particle Filter Housing with 1µm Particle Retention Filter – Pall Corporation type A/E

$\mathbf{J_V}$, $\mathbf{J_H}$ Custom-built adaptors with optical access - PMMA construction with an optical crown glass window, internal dimensions of 28 x 28 x 60 mm, two variations fitted with a silicone rubber seal where it meets the Nexthaler® Mouthpiece

K. Nexthaler® Device

L. Vertical Laser Sheet (see Section 2.3.2)

M. Nikkor 105mm macro lens

N. Photron APX RS High-speed camera

O. Front coated mirror 60 mm x 40 mm

$\mathbf{P_D}$, $\mathbf{P_u}$ Pressure Transducers – Kistler 4045A5 (25 mV/bar/mA sensitivity, natural frequency ≈ 80 kHz) used in conjunction with a National Instruments 6110 series data logger

Q. Fibre Optic Delivery of Laser Light

$\mathbf{R_c}$, $\mathbf{R_s}$, Cylindrical & Spherical Lenses

INSERT FIGURE 1 HERE

Figure 1: Schematic of Optical Diagnostics Test Rig

2.3.2 Test Rig Pneumatics Design Rationale and Operation

Figure 1 shows the pneumatics assembly within the test rig. Components A – J were linked by nylon hoses (ID 8 mm). The Nexthaler® device was positioned in a vertical orientation with suction applied, via the optical access adaptor J, in the same direction. This arrangement was defined by the needs of the experiment, but did not affect the operation of the device which is flow-dominated.

Although patients' inhalation profiles are individual and complex functions of time and inspiration (Kenyon *et al.*, 1999; Miller *et al.*, 2000), the transient air flow through a device can be more simply characterised in terms of the peak inhalation flow rate (Q_{max}), the total inhaled air volume, inhalation duration and flow rate acceleration, (Everhard *et al.*, 1997; Yakubu *et al*., 2013). Furthermore, many dry-powder inhalers emit the formulation rapidly from the device before completion of the initial flow acceleration phase of inspiration (Everhard *et al*., 1997; Burnell *et al.*, 1998; Finlay & Gehmlich, 2000). For our purpose of studying the phenomena of metered powder release, fluidisation and transport to the device mouthpiece, it was considered sufficient to generate controlled suction (inspiration) profiles up to the peak flow rate (Q_{max}) and ignore the subsequent tailing portion of the inspiration cycle, which is unlikely to contribute to the powder dose emission event. Air flow profiles selected for investigation with the test rig were set in terms of Q_{max} (40, 60 & 80 $l.min^{-1}$) and rise time, $t_{rise,}$ (0.3, 0.7 and 1.2 s) between initiation of suction and achievement of steady state pressure differentials, (P_U - P_D). These parameters are consistent with the majority of the *in vivo* inhalation profiles (peak inspiratory flow and time to peak inspiratory flow) reported for a cohort of 41 adult asthmatics through Nexthaler®, (Casaro *et al.,* 2014), and also enabled systematic variations of peak air flow rates and the initial rates of change of air flow with respect to time. Differential suction pressures across the Nexthaler® device were measured using a Kistler pressure transducer mounted in the optical adaptor (referencing the ambient pressure before suction). Simultaneous flow rate data were acquired by means of a thermal mass flow meter. This information was used to characterise the accelerating flow. Suction was produced by first evacuating the 20 litre vacuum vessel with the vacuum pump (A) to a pressure below 0.1 kPa and then isolating it using the ball valve (B). This entrapped vacuum generates the necessary pressure

205 differentials for suction periods up to 4 seconds without the requirement for a high-flow vacuum
206 pump. The pneumatic system comprises the following functional components. The interchangeable
207 orifice sonic flow restrictor, (D), prevents turbulent pressure variations at the device mouthpiece by
208 maintaining the ratio of downstream to upstream pressure across the restrictor < 0.5 for all flow
209 conditions. The setting of the flow control valve, (E), allows variation of Q_{max} from 40 to 80 $l.min^{-1}$.
210 The rapid switch on/off solenoid-controlled ball valve, (F), has minimal flow resistance when fully
211 open. Adjustment of the variable volume unit, (G), enables the rise time, t_{rise}, to be set between 0.3
212 and 1.2 s. The steady-state flow rate Q_{max} is monitored by the thermal mass flowmeter (H). The
213 1 µm particle filter, (I), collects fluidised powder and prevents deposition on the surfaces of the mass
214 flow meter and blockages further downstream.

215 The 20 l volume of the vacuum vessel was sufficiently large to maintain a pressure ratio of 0.5
216 across the sonic flow restrictor and ensure test durations between 0 and 4 seconds at the chosen
217 maximum value of flow rate. The pressure transducer, (P_U) mounted on the surface of the laser
218 illumination box measures the suction pressure at the Nexthaler® mouthpiece.

219

220 2.3.3 *Test Rig Optics for Imaging Events Within Nexthaler®*

221 High-speed imaging of the functionality of the dose protector mechanism and powder entrainment
222 from the dosing cup into the air stream was carried out by examining the region inside the device
223 where the metered dose of formulation is initially entrained by the air flow. A high-speed camera (N)
224 was used in conjunction with a copper-vapour laser light source (Type LS20-10, Oxford Lasers,
225 Oxford, UK). The laser light was directed to the image area by fibre-optic transmission as shown
226 schematically in Figures 2a & b. Light pulses of 25 ns duration, were synchronized with the camera
227 recording at 10,000 $frames.s^{-1}$ at a resolution set to 512 by 512 pixels, equivalent to an imaging
228 area approximately 5 mm by 5 mm. The imaging configuration utilised a 105 mm Nikkor macro-lens
229 with an aperture setting of f11 resulting in a pixel resolution limit of approximately 10 µm.

230

INSERT FIGURE 2 HERE

Figure 2. Schematic of Optical Equipment Set-up for Imaging Formulation Entrainment from Nexthaler® Metering Cup. (a), Side view, (b), Top view

2.3.4 Particle Plume Imaging & Flow Field Velocimetry at Nexthaler® Mouthpiece Exit

High-speed imaging of the particle plume at the exit of the device mouthpiece to investigate its temporal and spatial structure and two-dimensional high-speed velocity measurement of the ex-mouthpiece flow field using particle image velocimetry (PIV), were carried out using the experimental arrangement, shown schematically in Figures 3a-b.

INSERT FIGURE 3 HERE

Figure 3: Schematic of Optical Equipment Set-up used for Nexthaler® Ex-mouthpiece Plume Imaging and Particle Image Velocimetry Measurements. (a), Side view, (b), Top view

Here, the copper-vapour laser was replaced by a Pegasus dual-cavity neodymium-doped yttrium-lithium fluoride laser, Nd:YLF, (New-wave Research Inc. Fremont CA, USA), as the light source. This laser enabled illumination using either a single cavity, producing an even pulse separation time for use in the imaging work, or from both cavities, allowing the separation time between each cavity to be adjusted for the velocity measurement work. The light from the laser for the ex-mouthpiece work was formed into a light sheet using a spherical-cylindrical lens combination. The light sheet was directed so that it intersected the exit-plume from the device through the centre-line of the orifice, in-line with the flow direction. The high-speed imaging of the plume was carried out at a camera speed of 3000 frames.s^{-1} with a resolution of 1024 by 1024 pixels providing an imaging area 22 x 22 mm and pixel resolution of approximately 22 μm. This resolution limit is significantly larger

than the smallest particles in the flow; however, due to diffraction small particles appear much larger and cover more than one pixel in the image.

In order to investigate the temporal development of the air flow through the Nexthaler® DPI, particle image velocimetry was applied to the region of the flow near the exit of the mouthpiece. For these tests, the device was primed prior to suction but no powder was present. The particles used to trace the air flow, and thus provide the basis for velocity quantification, were olive oil droplets nominally 1 µm diameter, introduced into the air surrounding the Nexthaler® device via a six-jet atomiser (model 9306A TSI Instruments UK), and drawn through the device during the suction event. Olive oil particles were selected for their light-scattering properties and ability to enable accurate tracking of the local air-motion through the device even under highly turbulent conditions. The recorded particle images were analysed using DaVis software (LaVision GmbH) to calculate the flow-field velocity vectors.

PIV measurements utilised the same equipment set-up, but with the triggering of the laser and camera altered to create pairs of images. Each image pair had a short and controllable time separation (2-8 µs) between the first and second image, enabling calculation of particle velocity from their spatial displacement. Recording of the particle images was carried out at either 1000 or 2000 frames.s^{-1}, providing velocity`measurements at either 500 or 1000 vector fields per second, depending on the duration of the rise-time being examined.

3. Results and Discussion

3.1 Differential (Suction) Pressure Time Profiles

Figure 4 shows the differential pressure-time profiles recorded for eight flow rate, (Q_{max}) – rise time, (t_{rise}) combinations achieving steady state pressure differential. Due to limitations imposed by the design of the variable volume unit in the suction system, it was not possible to produce a dataset for a 0.3 s rise time with a 40 l.min^{-1} maximum flow rate. The profiles in the upper panels, (ai, aii, aiii),

were obtained using an unfilled Nexhaler® device; those in the lower panels, (bi, bii, biii), were obtained using a filled Nexthaler® with the metering cup primed by opening the device cover, (Corradi *et al.,* 2014). The shapes of the eight profiles in Figure 4 differ from those of Chavan & Dalby (2002), which show linear flow-time relationships during the flow acceleration phase until the steady state is achieved at Q_{max}. Such a relationship between flow rate and time is easy to describe mathematically, but involves a discontinuity in the flow acceleration at the changeover between the initial phase when the flow ramps up and the constant steady-state flow. Whilst a linear ramp profile may be suitable for quality assurance testing, it is well known that human inhalation profiles vary in a quasi-parabolic manner reaching a maximum before tailing.

INSERT FIGURE 4 HERE

Figure 4.: Effect of Variation in flow rate maximum and rise time on suction pressure-time profiles though Nexthaler® , (a) without powder loading but with metering cup primed, (b) with powder loading and metering cup primed. (green, red, blue traces; Q_{MAX} = 40, 60, 80 $l.min^{-1}$ respectively; vertical broken black lines delineate rise time set.).

In the present system, the initial portion of the profile is similar for each flow rate for a given rise time. Thereafter the differential pressure traces curve towards the steady state plateau. The theory of pneumatic circuits and transmission lines shows that this behaviour can be understood in terms of the inertance, capacitance and resistance of the test rig's circuit components and its fluid content. The traces confirm that independent variation of the peak flow rate Q_{max} and rise time of the suction profile has been achieved (i.e. the peak flow rate can be varied while maintaining a constant rise time), allowing a range of different flow profiles to be achieved.

Figures 4 (b) i–iii show that when the Nexthaler® device is filled and primed, and therefore with the dose-protector ready to be triggered by the breath-actuated mechanism on actuation, the resultant

307 pressure-differential profiles through the device differ slightly from those obtained with primed but
308 un-loaded devices, (Figures 4 (a) i-iii). The appearance of discontinuities (arrowed), indicates that a
309 change in the rate of change of pressure differential is induced by the resultant particle entrainment.

310

311 *3.2 Dose protector functionality and powder fluidisation*

312 Figure 5 presents high-speed images of the functionality of the dose protector mechanism and the
313 powder entrainment. The dosing (metering) cup shows as a circular region inside the bright grey
314 image of the bottom of the device, as seen through the circular mouthpiece orifice. The powder
315 dose is initially located in the centre of the dosing cup, where it shows as a white, granular region.
316 Under the test conditions shown, (Q_{max} 60 l.min $^{-1}$, 0.3 second rise time), the dose protector covers
317 the powder dose until 40 ms after the initiation of suction. Thereafter, the suction pressure
318 differential inside the Nexthaler® has built up sufficiently to trigger the breath-actuated mechanism,
319 which then displaces the dose protector to expose the metered powder to the air flow in the device's
320 swirl-chamber below the mouthpiece. The powder bed starts to rotate immediately, under the
321 influence of the developing vortex flow in the vicinity of the dosing cup. The bulk of the powder
322 dose is rapidly fluidised during the first phase of the interaction, which has a duration of around 20
323 ms after the dose protector is removed. A small proportion of the particles remains deeper inside
324 the dosing cup at this stage. This region is less exposed to the air flow and this powder remnant is,
325 therefore, fluidised much more gradually.

326

327 INSERT FIGURE 5 HERE

328

329 Figure 5: Images of dosing (metering) cup region showing powder fluidisation and dose protector
330 functionality. (Q_{max} 60 l.min^{-1}, rise time 0.3 s)

331

Particle fluidisation during this second phase appears to be stochastic. The aerodynamic forces are insufficient to pick up the large carrier particles, but the forces are fluctuating as a consequence of the high turbulence levels induced in the swirl chamber. Occasionally one or two particles are forced to move up towards the top edge of the dosing cup where they can be entrained by the flow and transported upwards via the swirl chamber to the mouthpiece. Under the prevailing experimental conditions, Figure 5 shows that the dosing cup is completely empty approximately 300 ms after the start of the flow.

3.3 Ex-mouthpiece aerosol plume - imaging

The imaging work carried out in section 3.2 has shown that after entrainment into the air flow, the powder is rapidly transported through the swirl chamber into the outlet tube towards the device mouthpiece. Within the swirl chamber high levels of swirl are induced by the internal flow passage geometry of the Nexthaler®. The air, and hence the particles, are expected to follow spiral paths with a large circumferential velocity component superposed on the upward axial velocity component towards the mouthpiece. The density of the lactose and drug solids is much higher than the air density, so the aerosol plume will be most dense near the surrounding walls, as can be seen in the image displayed in Figure 6. The large carrier particles experience a more pronounced outward displacement, whereas the fines are more uniformly distributed throughout the aerosol.

A typical single frame image of the emitted aerosolised particles, illuminated by the laser sheet positioned across the centreline of the mouthpiece, is shown in Figure 6. For clarity, this image and Figure 7 have been inverted, to show the particles in the light sheet as dark regions on a light background. The general appearance of the cloud suggests that the flow is highly agitated and turbulent, as confirmed by examination of the complete video. The larger particles in the placebo blend experience a more pronounced outward displacement whereas fines are more uniformly distributed. This is to be expected, since the design of the internal flow passage geometry of Nexthaler® induces a spiral path with a large circumferential velocity component superimposed on

the upward axial velocity component to the air drawn through the device by the inhalation manoeuvre, which is transmitted to the fluidised particles. The larger the particles, the greater the unit mass and the greater the centrifugal force imposed.

INSERT FIGURE 6 HERE

Figure 6: Typical Single Frame from High Speed Video Capture of Powder Emission from Nexthaler®: (Suction Conditions; Q_{max} = 60 l.min^{-1}, Rise Time = 0.3 s, Image captured at 0.062 s)

To characterise the temporal release of the powder from the device mouthpiece, the pixel intensities within a defined rectangle across the centre of the device mouthpiece, (Figure 6), were summed for each frame, ($\sum I_{Px}$). The individual $\sum I_{PX}$ values for a given frame were then normalised against the maximum value obtained in the entire ensemble of frames in the video from the start to the end of suction pertaining to that single dose powder discharge from the Nexthaler® unit. Plotting the normalised intensities against time, (Figure 7) thus provides a quantitative description of the powder emission kinetics. Normalising the summed intensities in this manner allows quantitative comparison of the effects of Q_{max} and rise time on the powder emission kinetics by eliminating the influences of intra-device variations of unit dose metering and temporal variation in laser pulse energy.

Figure 7a compares the pressure differential (pressure drop, ΔP), generated across the Nexthaler® with the normalised intensity profiles of powder emission during the air flow acceleration phase of an event over a rise time of 0.3 s resulting in a steady-state flow rate, (Q_{max}), of 60 l.min^{-1}. Figure 7b presents a selection of (inverted) particle images captured between 30 - 130 ms after commencement of flow, with the corresponding acquisition time indicated on each frame and its

location on the abscissa of Figure 7a. The normalised intensity profiles suggest that powder emission takes place in four phases characterised by:

(i) a small peak (A), normalised intensity ~0.2 around 40 ms,

(ii) a large peak (B), normalised intensity maximum 1.0 around 60 - 70 ms, which is associated with most of the powder emission,

(iii) a second small peak (C), normalised intensity maximum ~ 0.3 around 80 ms, followed by,

(iv) a slow decline in normalised intensity, (D), over 90 – 300 ms with some minor spikes commensurate with the emission of small bursts of fine particles and a few larger aggregates, (see Figure 7b, e.g. Frame 642).

Imaging of the dosing cup region, (see section 3.2 figure 5), showed that the bulk of the powder entrainment takes place between 40 and 60 ms. The time required to transport the powder from the dosing cup to the mouthpiece exit explains the delay in appearance of the large intensity peak B, (Figure 7), at 60-70 ms. The pressure differential across the Nexthaler®, (Figure 7a), shows a discontinuity coinciding with the large intensity peak B; equivalent discontinuities for powder-filled devices are also shown in figures 4b(i –iii). These can be attributed to the substantial amounts of flow energy required to lift the particles from the dosing cup to the mouthpiece and the increased energy dissipation associated turbulent multi-phase flows. The particle intensity images, (Figure 7b), also show that peak C, around 80 ms, is linked with the emission of large particles, or aggregates which are heavier and will therefore be held up inside the device for a longer period of time than the finer material. Finally, it should be noted that a small quantity of finer particles is visible in the images taken at 30 and 40 ms, times when the dose protector still covers the powder dose. Careful inspection of high-speed images of the dosing cup region reveals that some air flows through a narrow gap created by a small uplift of the dose protector due to the build-up of suction in this region. This air flow succeeds in dislodging some of the fine material and initiating premature release. However, as evidenced by the normalised intensity profile peak areas, (A relative to B+C), the total amount of this premature emission is very small compared with the release of the majority of the powder dose.

INSERT FIGURE 7 HERE

PLEASE ROTATE LEFT

To examine the effect of the flow conditions on powder dose emission, the temporal behaviour of the normalised intensity profiles was compared across all the test conditions used in this study. Figures 8a-c show the profiles with rise time of 0.3, 0.7 and 1.2 s, respectively. All three plots show the time to achieve peak value, (1.0), of normalised-intensity, (t_{max}), increases with increase in rise time, but decreases with increase in Q_{max}, confirming that flow rate acceleration controls powder emission rate. The width of the main intensity peak, measured from the point of rapid increase in intensity gradient between peaks A and B to the point of inflection between peaks B and C, increases from about 15 ms to 25 ms as the rise time increases from 0.3 s to 1.2 s. However, the peak width changes little with flow rate, i.e. for the 1.2 s rise time case, the peaks are all between 23 and 25 ms.

The early, small peak (i.e. Peak A in Figure 7) occurs 40-50 ms after the suction is switched on for all test conditions, before movement of the dose protector was observed in the high-speed images. As noted earlier, the small quantity of fines emission at this stage will occur as soon as a narrow flow path underneath the dose protector admits sufficient air to pick up fines from the powder dose. However, the intensity data demonstrates the magnitude of this early peak diminishes with increasing rise time.

Comparison of the pressure and image-intensity traces shown in figure 7 clearly demonstrates that the small discontinuity found in the differential-pressure trace coincides with the start of the large peak in normalised plume-intensity (peak B). This coincidence is also found in all of the traces detailed in figures 4 and 8, which supports the view that the pressure discontinuities are associated with the release of the powder-dose into the flow, not the initiation of dose protector movement. The

delay in the dose-protector movement relative to the start of suction, and hence dose-release, is dependent on the suction profile and as such varies with both max flow-rate and rise-time. The design of the Nexthaler® DPI is such that the dose protector should withdraw when a pre-set suction of 2 kPa below ambient is reached; comparison of event timings in Figures 4, 5 and 7 shows that the dose is consistently emitted very shortly after sufficient suction occurs to move the dose protector. Figure 4 suggests that, for cases where the peak flow rate is 40 $l.min^{-1}$, the actual trigger point of the dose protector is slightly below 2 kPa. This pressure differential is very close to the limit of device actuation, which explains why the time from the start of the event flow to the main normalised intensity peak (shown in figure 8) is much longer than at peak flow rates of 60 and 80 $l.min^{-1}$. Achieving a high peak flow rate or a short rise time, on the other hand, requires a large rate of change of pressure. Inertia of the dose protector and the powder dose will tend to resist rapid movements somewhat, consequently suction pressures just above 2 kPa are needed to achieve dose protector movement and powder release at 60 and 80 $l.min^{-1}$ flow rates and shorter rise-time (also see Figure 4).

INSERT FIGURE 8 HERE

Figure 8 – Normalised intensity profiles as function of time for flow conditions: peak flow rate 40 $l.min^{-1}$ (green traces), 60 $l.min^{-1}$ (red traces) and 80 $l.min^{-1}$ (Blue traces). Rise time: (a) 0.3 s, (b) 0.7 s, (c) 1.2 s

458 3.4 *Ex-mo*uthpiece aerosol plume - Particle image velocimetry

459 Axial and radial velocity components were measured across a plane perpendicular to the device
460 exit, along the centreline of the mouthpiece. The measurement region is 20 mm x 20 mm in size,
461 with single vectors calculated over interrogation regions approximately 0.6 mm x 0.6 mm; 50%
462 overlap of the interrogation regions provided a vector spacing of 0.3 mm across the field. An
463 example of a typical vector field is shown in Figure 9 for the flow conditions Q_{max} 60 l.min^{-1}, rise time,
464 0.3 s; the magnitude of the flow velocity is indicated by means of the colour scale. The maximum
465 velocity of 40 m.s^{-1} is coloured white.and appears around radius $\pm$5 mm just outside the
466 mouthpiece.

467 A slight asymmetry is evident with somewhat larger region of high velocity on the right hand side of
468 the velocity field images (see figure 10b). If, as surmised earlier, the air follows spiral paths inside
469 the device and develops concentrated regions of high-speed flow at the periphery, this accounts for
470 the reverse flow in evidence around the centreline of the mouthpiece exit, (see Figure 9 near the red
471 line at radius zero). This is a well-known secondary flow pattern at high swirl levels, which
472 generates high shear in the internal flow passages. After exiting the mouthpiece, the unbalanced
473 centrifugal force on the rotating flow causes the fastest fluid to move radially outwards. The flow
474 interacts with the stationary surroundings, which generates additional shear stress on the external
475 flow, which in turn causes turbulent eddies, several of which are clearly visible in Figure 9.

476

INSERT FIGURE 9 HERE

Figure 9 – Typical PIV vector field with analysis line position, Q max = 60 l.min^{-1} t_{rise} = 0.3 s, 0.23 s after start of suction (arrows indicate 2D direction of flow)

Quantitative information was extracted from the 2D vector flow fields by calculating a mean axial velocity component ($\overline{V}$) as follows:

$$\overline{V} = \sum_i V_i \Delta A_i / A_L \ ,$$

where V_i = velocity at location i, ΔA_i = area of the image plane used in the velocity measurement at location *i*, A_L = total area used for the velocity measurements that intersect the analysis line; points *i* are spaced uniformly along a line parallel to the device exit orifice (red line in Figure 9).

Since turbulent eddies cause large instantaneous variations in the local axial velocity, smoothed $\overline{V}$ values are reported, to produce more meaningful data. These were computed using a shifting time average over ten vector fields, corresponding to an averaging time of 10 ms.

Figure 10a shows smoothed mean axial velocity-time profiles obtained for Nexthaler® during the flow acceleration phase with the same flow conditions as the high-speed imaging tests reported above (section 3.3, Figure 7) i.e. steady-state air flow rate conditions Q_{max}, 60 l.min^{-1}, rise time 0.3s along with the recorded differential pressure. It should be noted that the averaging of these axial velocity components along the analysis line (see figure 9) does not exactly represent the mean axial flow velocity at the device-exit since the analysis line was extended beyond the 8 mm diameter mouthpiece (figure 9) to off-set the turbulent and spreading nature of the post-orifice flow and only represents the narrow section of flow illuminated by the laser sheet. However, the increase of the

503 mean velocity is found to correlate well with the decrease of the measured pressure differential,
504 suggesting that the post-processed average axial velocity across the sample line (shown in figure
505 10) is a good indication of the general changes of the flow rate of the air drawn through the device
506 as a function of time.

507 Figure 10b presents a selection of PIV velocity vector fields with the corresponding time indicated
508 on each frame as well as the location on the time axis. The velocity scale is the same for all
509 images, white corresponding to 40 $m.s^{-1}$ and dark blue to zero $m.s^{-1}$, respectively. The maximum
510 value is clearly lower in the first image (25ms) when flow rate is still increasing, but otherwise the
511 PIV images show the same flow features noted earlier for Figure 9 with flow asymmetry toward the
512 right of the images, possibly induced by the internal flow paths within the Nexthaler® device.
513

514 INSERT FIGURE 10 HERE

515 **PLEASE ROTATE LEFT**

516

517 **4. Conclusions**

518 In this study, we have successfully applied optical diagnostics to characterise various aspects of the
519 Nexthaler® DPI and demonstrated how detailed information about the device functionality and
520 powder dose emission can be obtained by means of these techniques.

521 Results from the study have shown that fluidisation of the bulk of the powder occurred shortly after
522 the withdrawal of the dose protector. Powder was found to arrive at the mouthpiece exit after a
523 short delay due to transport of the powder from the dosing cup to the mouthpiece exit by the air
524 stream. The powder dose is mainly emitted in a short burst, which occurs after the withdrawal of the
525 dose protector, with a duration between 15 and 40 ms, dependent upon Q_{max} and rise time (flow rate
526 acceleration). Thereafter there is an emission of larger particles with residual fine material for a
527 further 100 - 150 ms. Most of the powder dose has been aerosolised within 100ms of flow initiation.

The visualisation study also revealed that a small fraction of the fines is emitted whilst the dose protector still covers the dosing cup.

High-speed imaging studies have shown that a highly turbulent, rotating flow is created in the internal passages of Nexthaler®. These high swirl levels generate a highly sheared, turbulent flow inside the device, which interacts with the stationary surrounding air just outside the mouthpiece generating additional turbulence within the emitted plume. Moreover, the centrifugal force flings the larger carrier particles radially outwards towards the walls of the internal passages increasing the probability of wall impacts.

References

- Acerbi D., Brambilla G., Lewis D., Meakin B. (2007). 'Gaining approval to market therapeutically equivalent inhalers in the EU: an industry perspective', Proc. Respiratory Drug Delivery Europe pp. 127-140.
- de Boer A.H., Gjaltema D., Hagedoorn P. (1996). 'Inhalation characteristics and their effects on in-vitro drug delivery from dry powder inhalers. Part 2: effects of peak flow rate (PFIR) and inspiration time on the in-vitro drug release from there different types of commercial dry powder inhalers', International Journal of Pharmaceutics, Vol. 138, pp. 45-56.
- British National Formulary 68, (2014). Section 3. Respiratory System, pp. 180-201.
- Burnell P.K.P, Grant A.C., Haywood P.A., Prime D., Sumby B.S., (1998). 'Powder inhalers – exploring the limits of performance', Respiratory Drug Delivery VI, pp. 259-266.
- Casaro D., Brambilla G., Pasquali I., Sisti V., (2014). 'In vitro aerosol performances of NEXThaler® using representative inhalation profiles from asthmatic patients', Proceedings of Respiratory Drug Delivery 2014. Vol. 2, pp. 375-380.
- Chavan V. and Dalby R. (2002). 'Novel system to investigate the effects of inhaled volume and rates of rise in simulated inspiratory air flow on fine particle output from a dry powder inhaler', AAPS Pharmaceutical Science and Technology, Vol. 4, No. 2, pp. 1-6.
- Church T.K., Brambilla G., Lewis D.A., Meakin B.J., Poli G. (2010), 'Sub-micron particles: an effective menas of achieving bronchodilation' Proc. Respiratory Drug Delivery, Vol 2 pp 509-512
- Clark A.R. and Hollingsworth A.M. (1993). 'The relationship between powder inhaler resistance and peak inspiratory conditions in healthy volunteers: implications for in-vitro testing', Journal of Aerosol Medicine, Vol. 6, pp. 99-110.
- Corradi M., Chrystyn H., Cosio B.G., Pirozynski M., Loukides S., Louis R., Spinola M., Usmani O.S. (2014). 'NEXThaler, an innovative dry powder inhaler delivering an extrafine fixed combination of beclometasone and formoterol to treat large and small airways in asthma', Expert Opinion on Drug Delivery, Vol. 11, No. 9, pp. 1497-1506.

- Dunbar C.A., Hickey A.J. and Holzner P. (1998). 'Dispersion and characterization of pharmaceutical dry powder aerosols', KONA Powder and Particle, Vol. 16, pp. 7-45
- Electronic Medicines Compendium, Accessed August 2015.
- Everard, M.I., Devadason, S.G., Le Souef, P.N. (1997). 'Flow early in the inspiratory manoeuvre affects the aerosol particle size distribution from a Turbuhaler'. Respiratory Medicine, Vol. 91, pp. 624-628.
- Finlay W.H. (2001), '*The mechanics of inhaled pharmaceutical aerosols – an introduction*', Academic Press, San Diego.
- Finlay W.H. and Gehmlich M.G., (2000). 'Inertial sizing of aerosol inhaled from two dry powder inhalers with realistic breath patterns versus constant flow rates', International Journal of Pharmaceutics, Vol. 210, pp. 83-95.
- Friebel, C., Steckel, H., Muller, B.W. (2012). Rational design of a dry powder inhaler: device design and optimization. Journal of Pharmacy and Pharmacology, Vol. 64, pp. 1303–1315.
- Hawksworth, G.M., James, I., Chrystyn, H., (2000). 'Characterization of the inspiratory manoeuvre when asthmatics inhale through a Turbohaler pre- and post-counselling in a community pharmacy'. Respiratory Medicine, Vol. 94, pp. 501-504.
- Hindle M. and Byron P.R. (1995). 'Dose emission from marketed dry powder inhalers', International Journal of Pharmaceutics, Vol. 116, pp. 169-177.
- Kuna P., Mirco G., Lucci G., Scuri M., Acerbi D., Iwona S. (2015). 'Pharmacokinetics and pharmacodynamics of an extrafine fixed pMDI combination of beclometasone dipropionate/formoterol fumarate in adolescent asthma', British Journal of Clinical Pharmacology, Vol 79 pp 1365-2125.
- Kenyon D., Schenkel E., Miller D., Angelini B., Skoner D. (1999). 'Assessment of inspiratory flow rates and rise time data in patients with asthma', European Respiratory Journal, Vol. 14, pp. 525s.
- Laube B.L., Janssens H.M., de Jongh F.H.C., Devadason S.G., Dhand R., Diot P., Everard M.L., Horvath I., Navalesi P., Vosbaar T. and Chrystyn H. (2011). 'ERS/ISAM task force

591 consensus statement: recommendations on what pulmonary specialist should know about
592 the new inhalation therapies, European Respiratory Journal, Vol. 37, pp. 1308-1331.
593 • Miller D., Schenkel E., Kenyon D., Harrison J. (2000). 'Airflow profiles and inhaler technique
594 with the new mometasone furoate dry powder inhaler (MF-DPI)', Journal of Allergy and
595 Clinical Immunology, Vol 105, pp. S16.
596 • Newman S.P. and Busse W.W. (2002). 'Evolution of dry powder inhaler design, formulation
597 and performance', Respiratory Medicine, Vol. 96, 293-304.
598 • Ngoc NTQ, Chang L, Jia X, Lau R (2013). 'Experimental investigation of design parameters
599 on dry powder inhaler performance', International Journal of Pharmaceutics, Vol 457, pp. 92-
600 100.
601 • Pasquali I., Brambilla G., Long E.J., Hargrave G.K. and Versteeg H.K. (2012). 'A
602 visualisation study for the aerosol generation in NEXThaler®', Poster abstract MN-1150,
603 Proceedings AAPS Conference, October 2012, Chicago, IL.
604 • Physicians' Desk Reference 2015. PDR eBook
605 • Staniforth J.N. (1995) 'Performance-Modifying Influences in Dry Powder Inhalation Systems',
606 Aerosol Science and Technology, Vol. 22, No. 4, pp. 346-353
607 • Sweeney L.G. and Finlay W.H. (2007). 'Lift and drag forces on a sphere attached to a wall in
608 a Blasius boundary layer', Journal of Aerosol Science, Vol. 38, pp. 131-135.
609 • Voss, A., Finlay, W.H. (2002). 'Deagglomeration of dry powder pharmaceutical aerosols'.
610 International Journal of Pharmaceutics, Vol. 248, pp. 39–50.
611 • Wang Z., Lange C.F. and Finlay W.H. (2004). 'Use of an impinging jet for dispersion of dry
612 powder inhalation aerosols', International Journal of Pharmaceutics, Vol. 275, pp. 123-131.
613 • Xu Z., Mansour H.M., Mulder T., McLean R., Langridge J. and Hickey A.J. (2010).
614 'Heterogeneous particle deaggregation and its implication for therapeutic aerosol
615 performance', Journal of Pharmaceutical Sciences, Vol. 99, pp. 3442-3461.

- Xu Z. and Hickey A.J. (2013). ‘A comparison of aerosol performance using standardized entrainment tubes vs. dry powder inhaler devices’ KONA Journal of Powder and Particle Technology, Vol. 30, pp. 201-210.
- Yakubu S.N., Assi K.H., Chrystyn H. (2013). ‘Aerodynamic dose emission characteristics of dry powder inhalers using Andersen Cascade Impactor with a mixing inlet: The influence of flow and volume’, International Journal of Pharmaceutics, Vol. 455, pp. 213-218.
- Zhou Q.T, Armstrong B., Larson I., Stewart P.J., Morton D.A.V. (2010). ‘Understanding the influence of powder flowability, fluidization and de-agglomeration characteristics on the aerosolization of pharmaceutical model powders’, European Journal of Pharmaceutical Sciences, Vol. 40, pp. 412–421.

*Graphical Abstract (for review)

GRAPHICAL ABSTRACT

OF

Optical diagnostics study of air flow and powder fluidisation in Nexthaler®

Part I: Studies with Lactose Placebo Formulation

Pasquali I.[1], Merusi C.[1], Brambilla G.[1], Long E.J.[2], Hargrave G.K.[2], Versteeg H.K.[2†]

[1]ChiesiFarmaceuticiS.p.A., Parma, Italy

[2]Wolfson School of Mechanical and Manufacturing Engineering, Loughborough University, Loughborough, United Kingdom

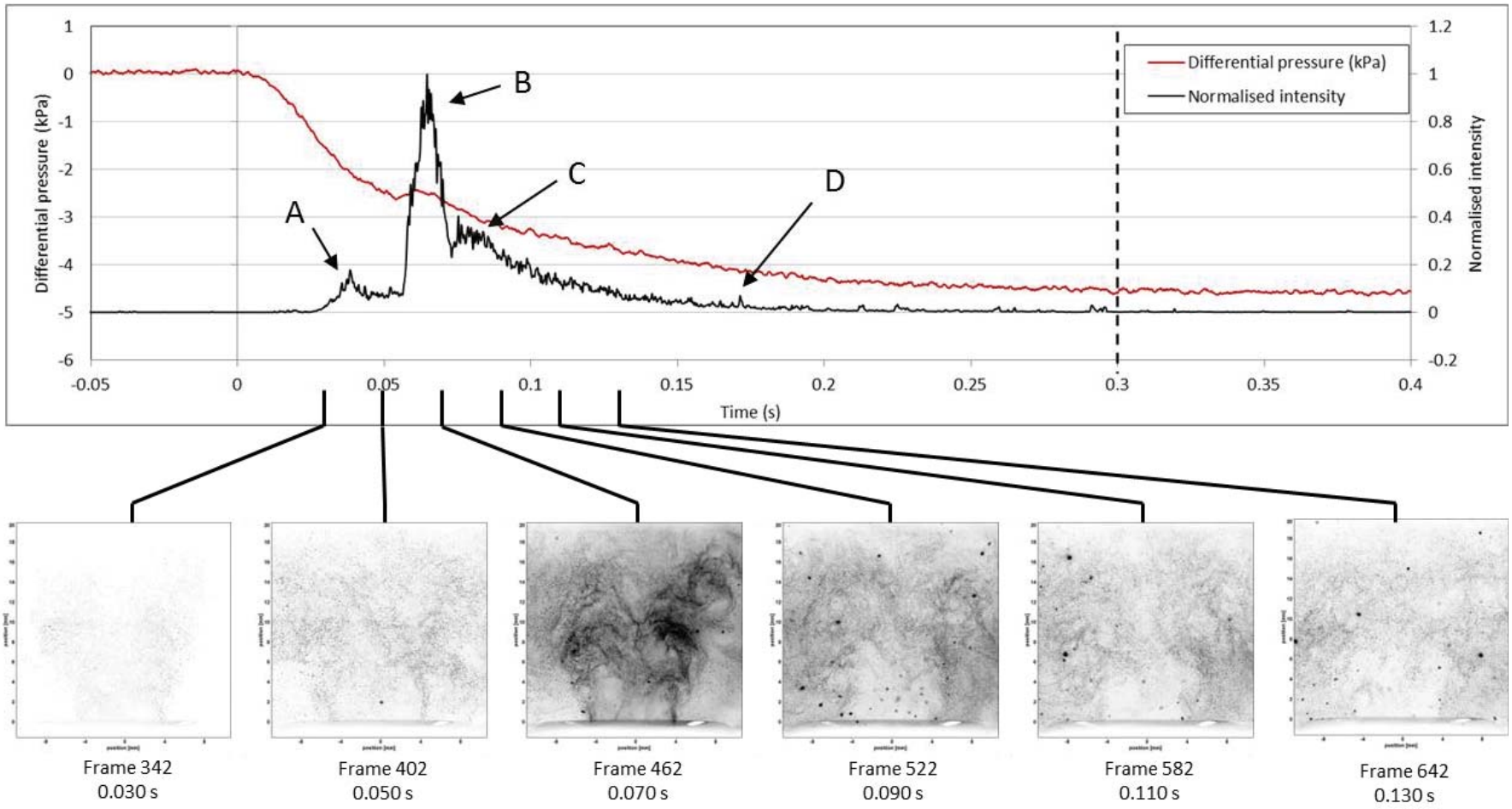
Differential pressure (kPa)
Normalised intensity
Time (s)
A
B
C
D
Frame 342
0.030 s
Frame 402
0.050 s
Frame 462
0.070 s
Frame 522
0.090 s
Frame 582
0.110 s
Frame 642
0.130 s

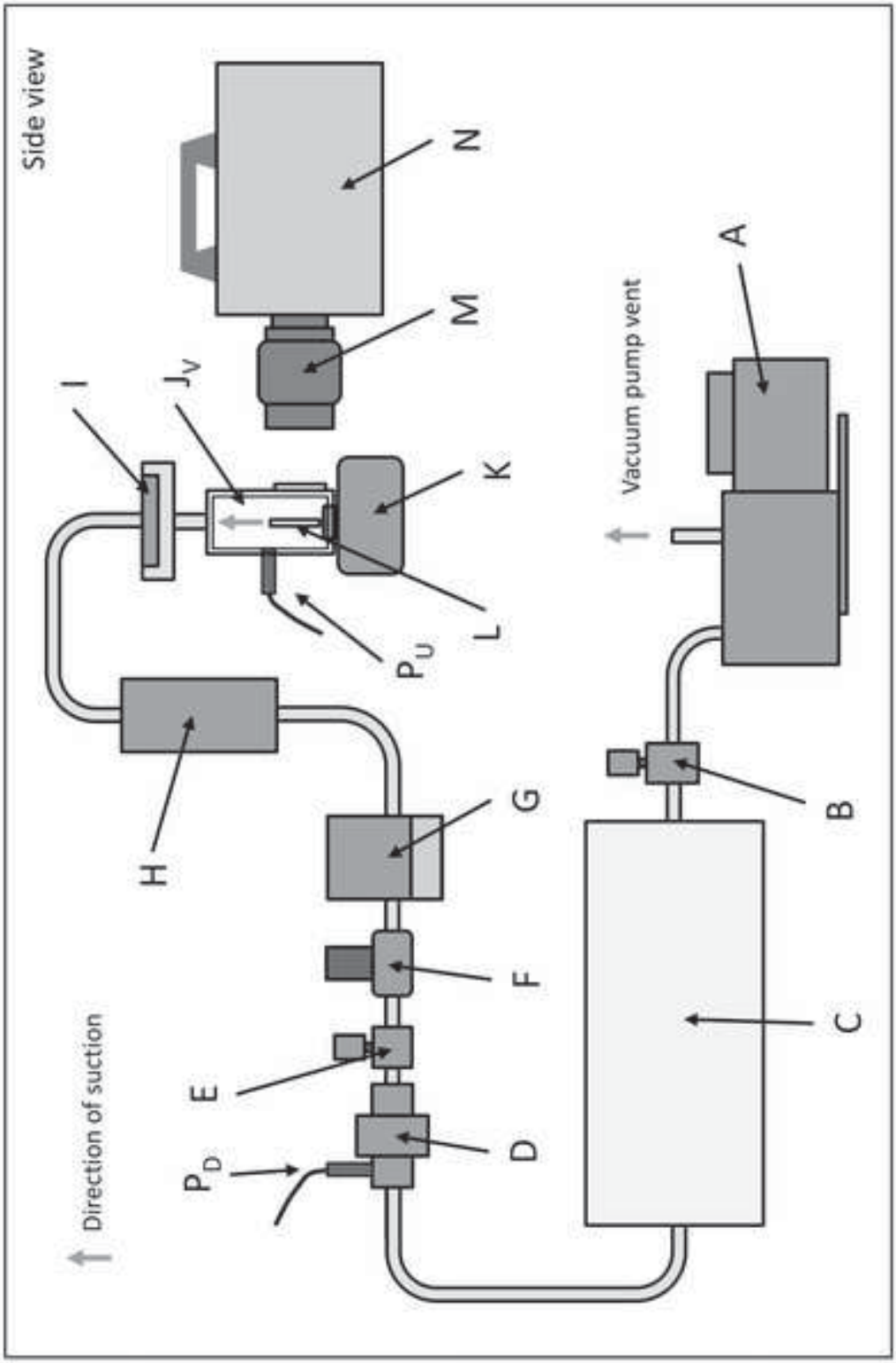

Figure 1

Figure(s)

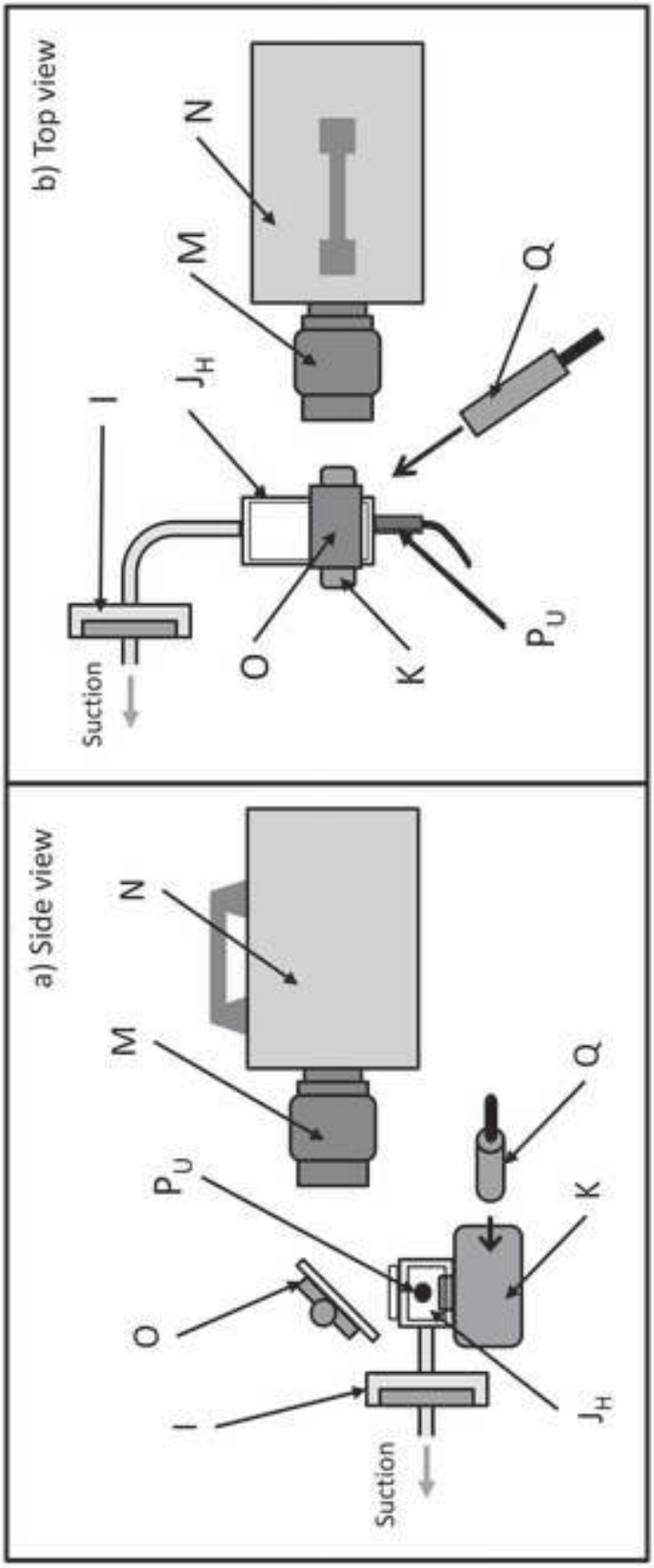

Figure 2

Figure(s)

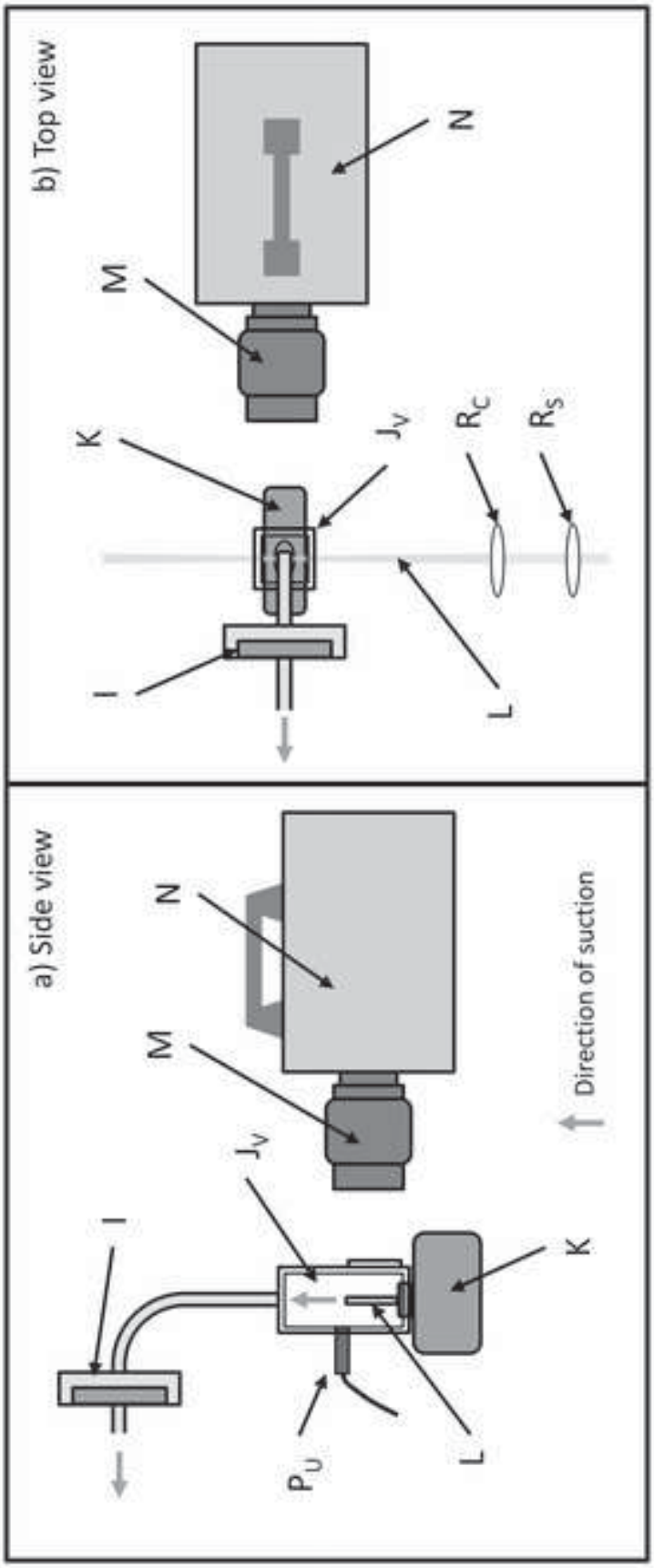

Figure 3

Figure(s)

Figure(s)

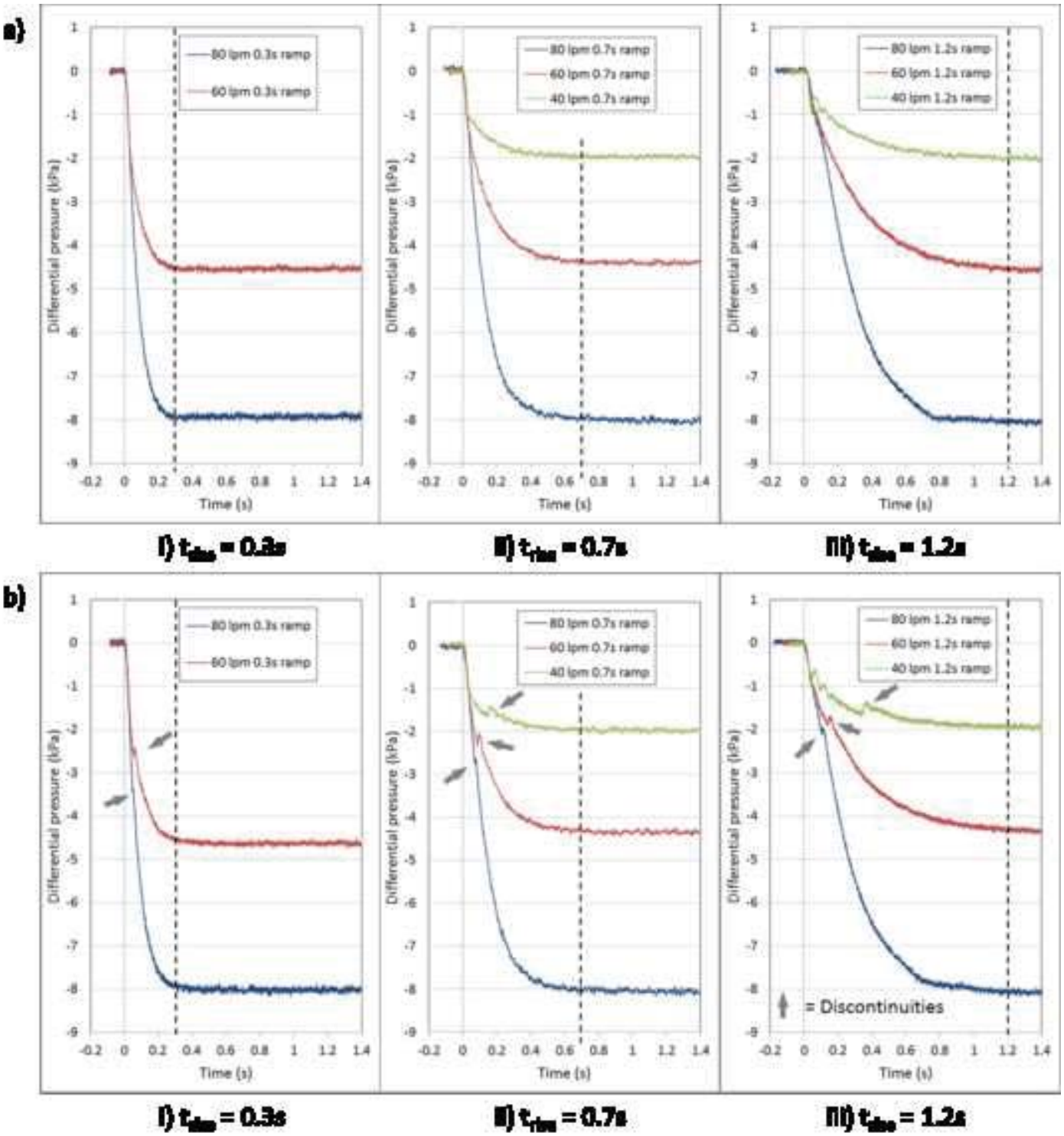

Figure 4

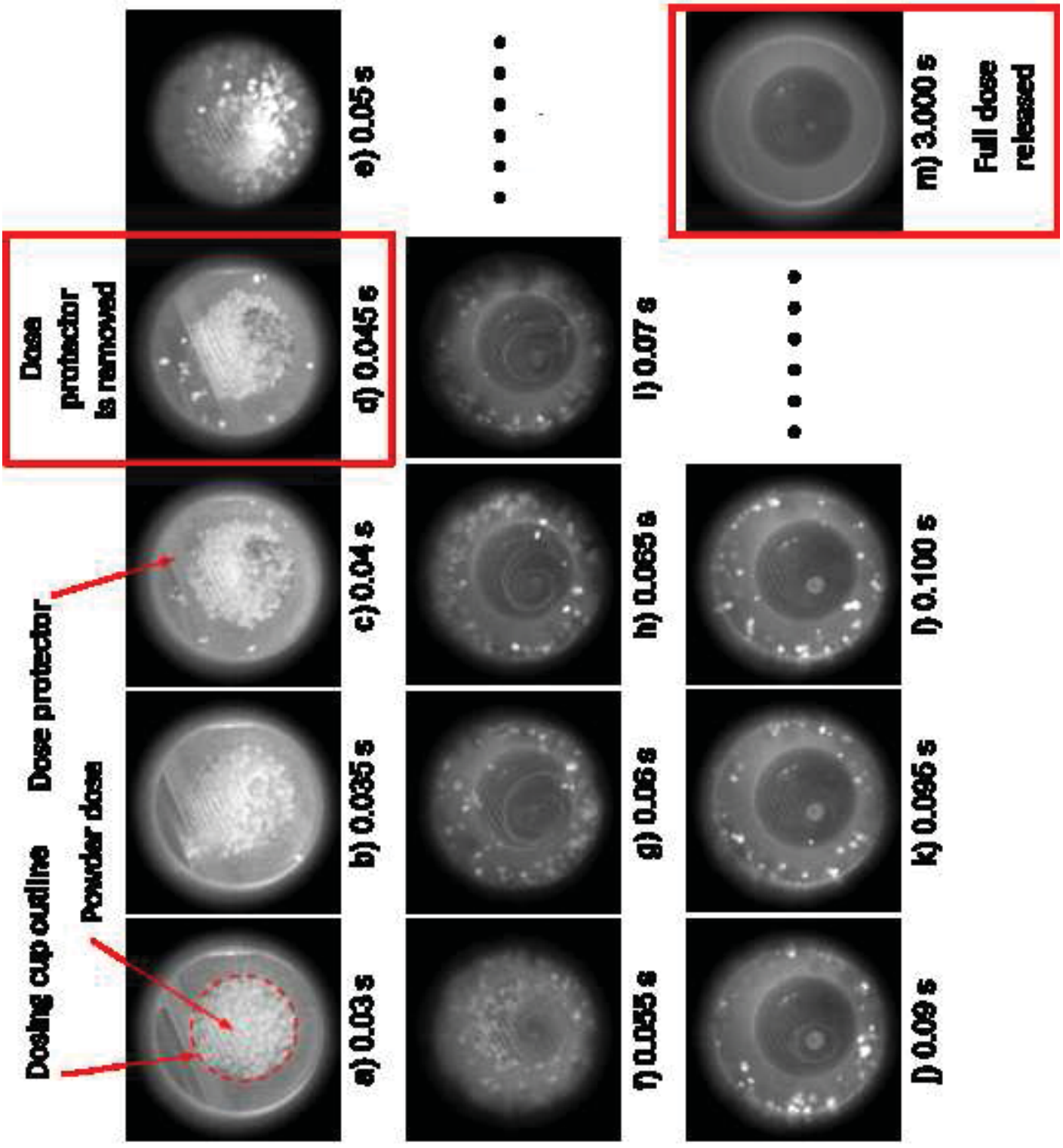

Figure 5

Figure(s)

Figure 6

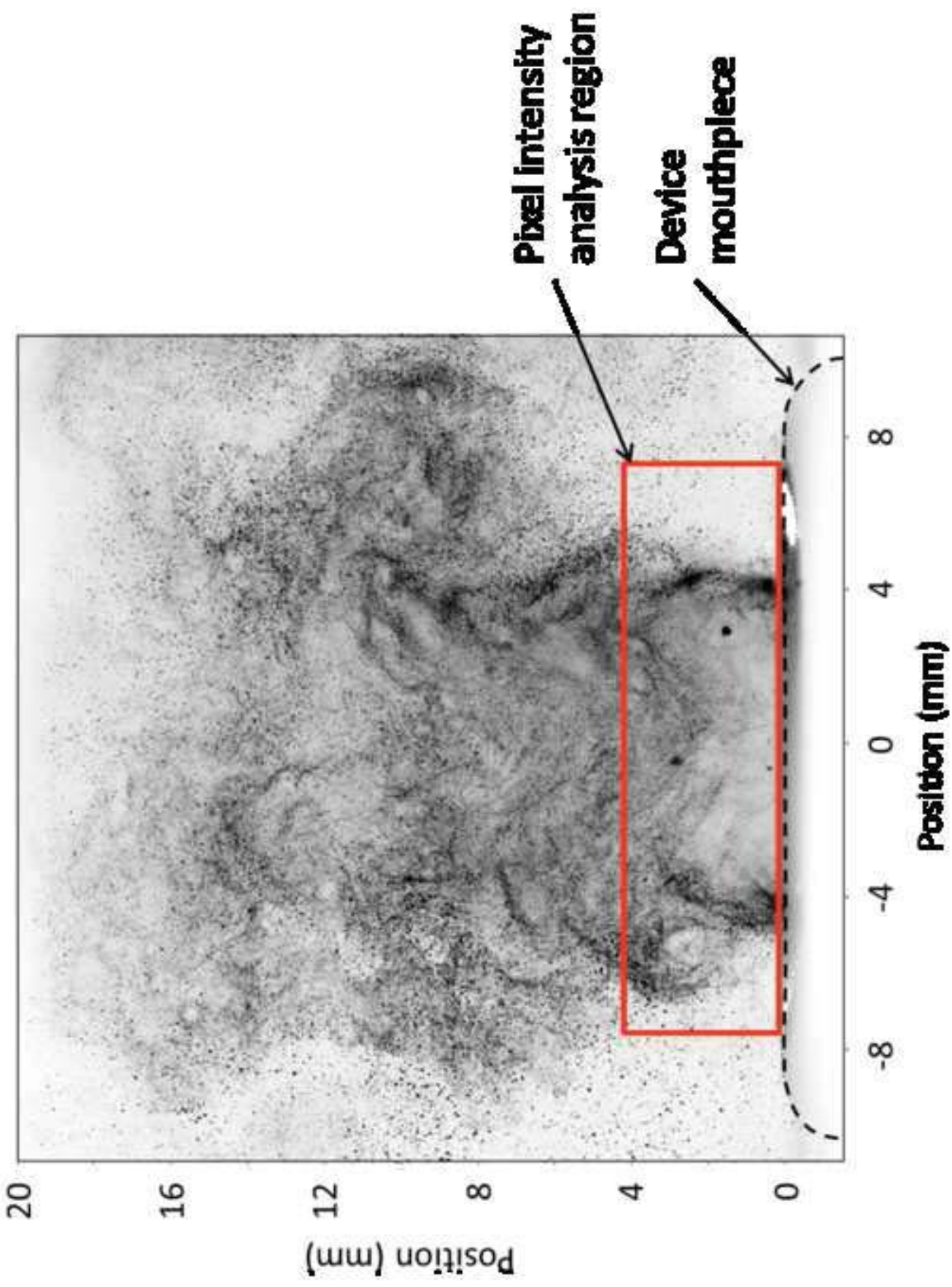

Figure(s)

Figure(s)

Figure 7

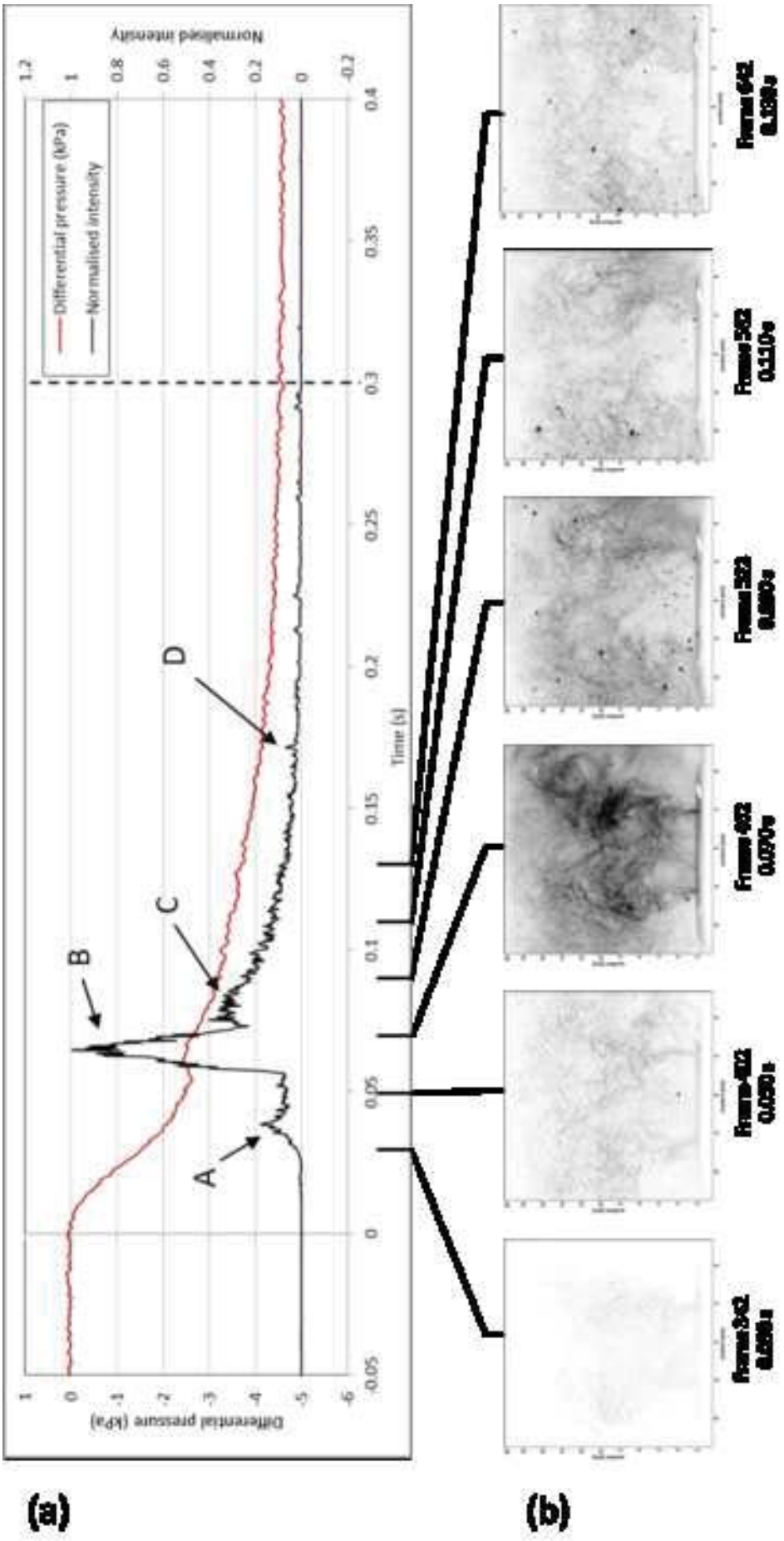

Figure 7

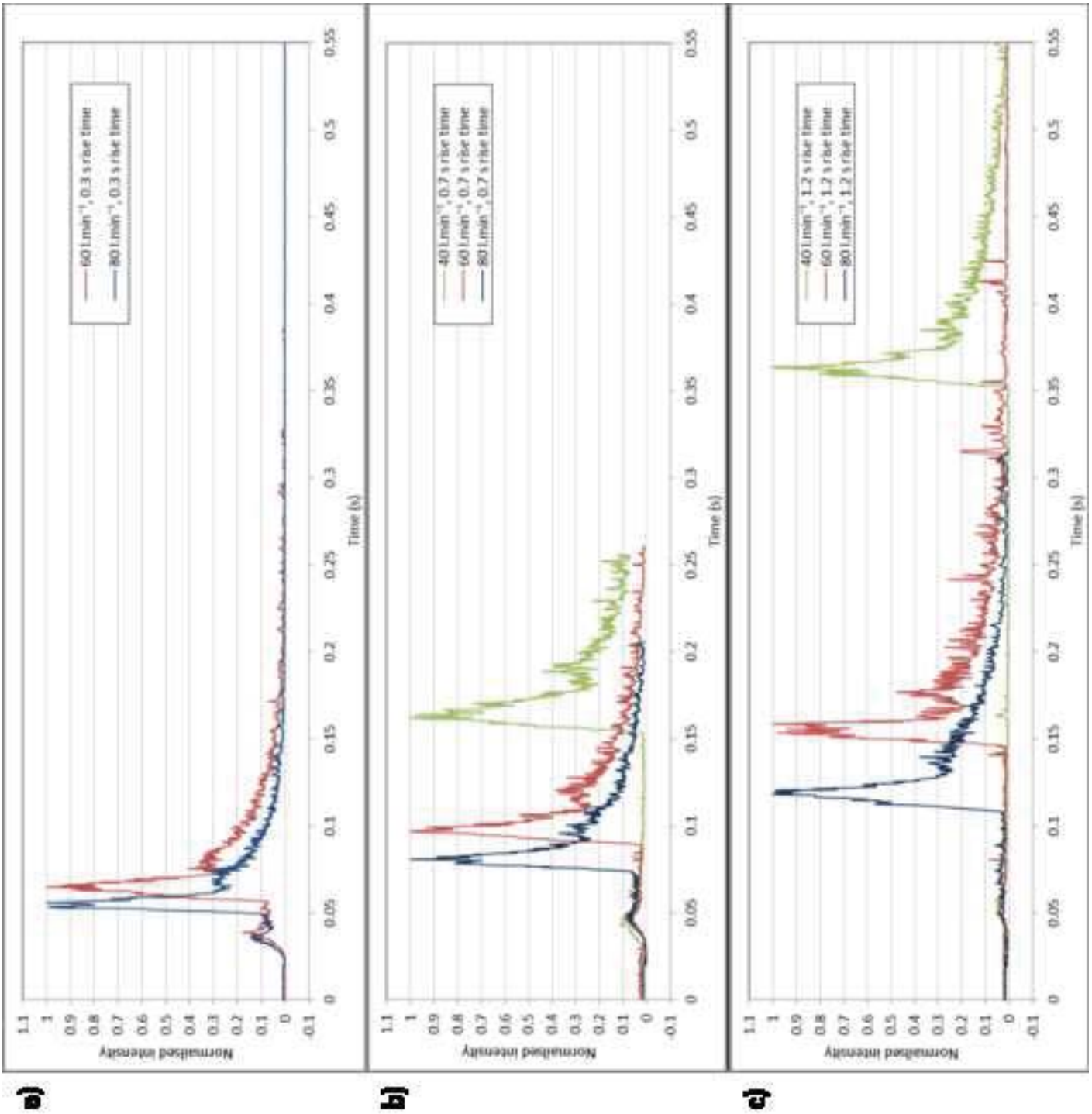

Figure 8

Figure(s)

Figure(s)

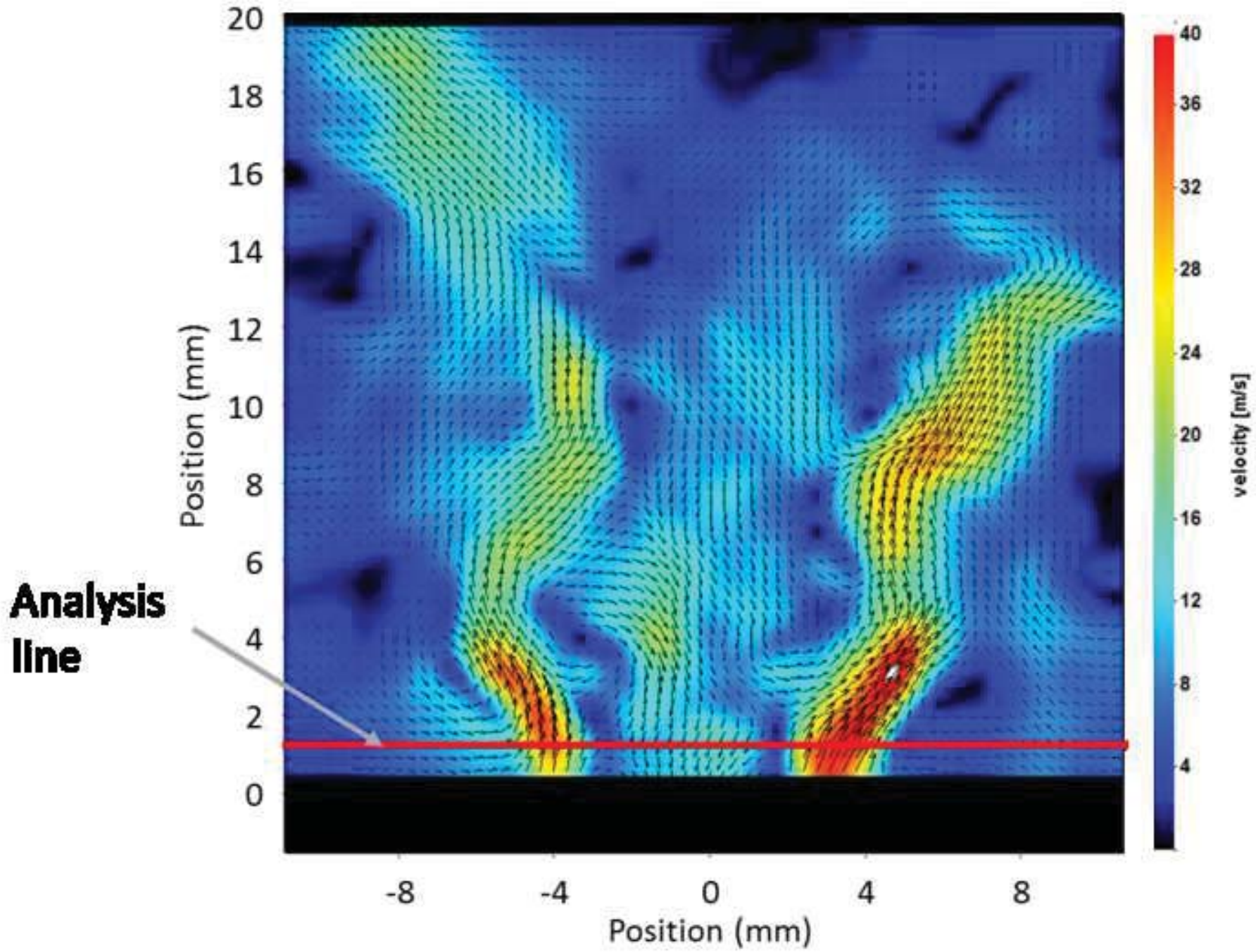

Figure 9

Figure(s)

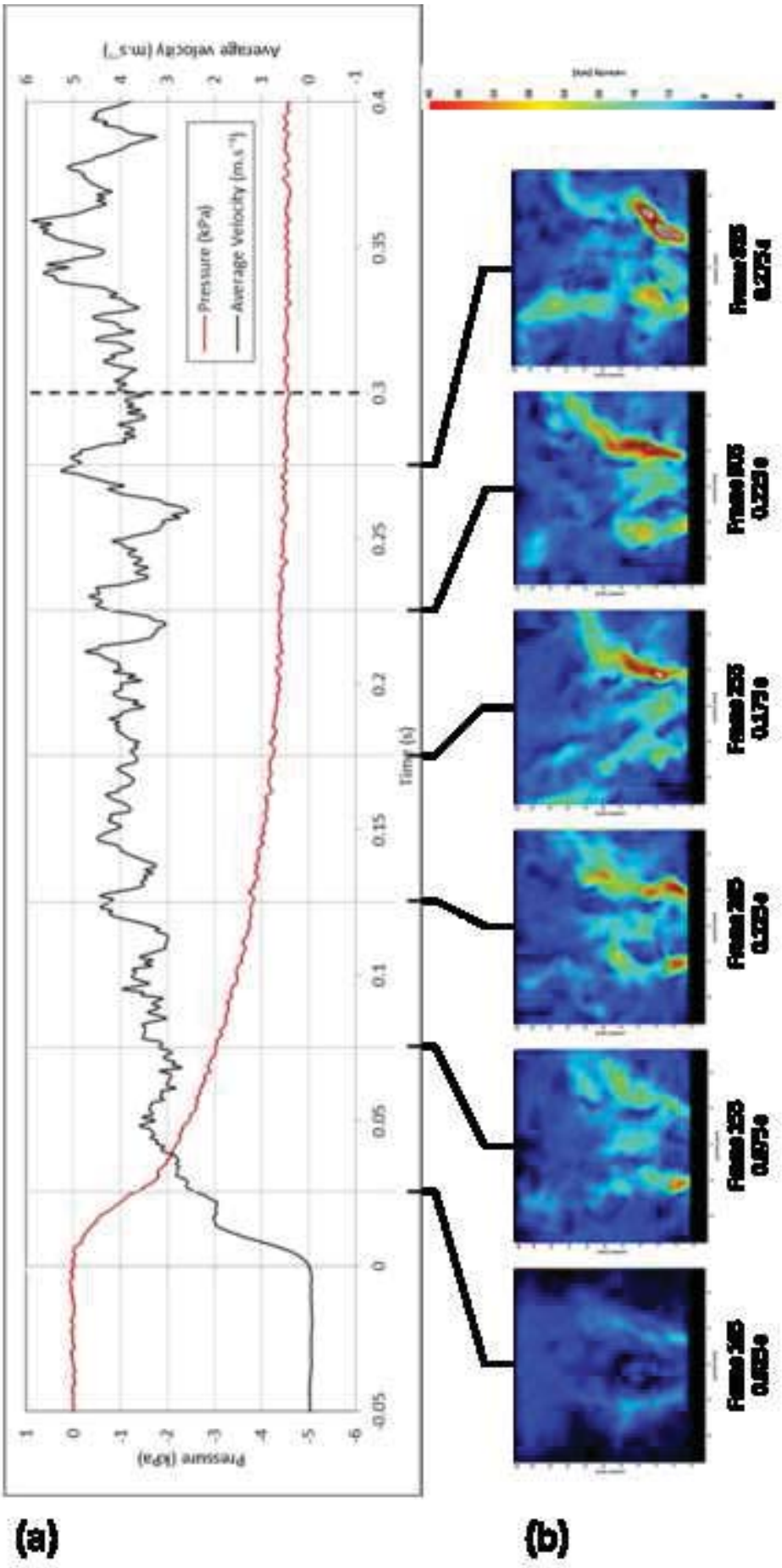

Figure 10